MOIRÉ PATTERNS FROM A CCD CAMERA
Are They Annoying Artifacts or Can They be Useful?

Tong Tu and Wooi-Boon Goh
School of Computer Engineering, Nanyang Technological University, Singapore 639798, Singapore

Keywords: Moiré pattern analysis, Image-based metrology, Surface reconstruction.

Abstract: When repetitive high frequency patterns appear in the view of a charge-coupled device (CCD) camera, annoying low frequency Moiré patterns are often observed. This paper demonstrates that such Moiré pattern can useful in measuring surface deformation and displacement. What is required, in our case, is that the surface in question is textured with appropriately aligned black and white line gratings and this surface is imaged using a grey scaled CCD camera. The characteristics of the observed Moiré patterns are described along with a spatial domain model-fitting algorithm that is able to extract a dense camera-to-surface displacement measures. The experimental results discuss the reconstruction of planar incline and curved surfaces using only a coarse 33 lines per inch line grating patterns printed from a 600 dpi printer.

1 INTRODUCTION

Moiré patterns are the results of the interference fringes produced by superimposing two sets of repetitive gratings. These patterns are used in metrology for tasks such as strain measurements, vibration analysis and the 3D surface reconstruction (Kafri, 1990), (Walker, 2004), (Creath, 2007). Moiré images are normally obtained using a camera to capture the patterns generated by superimposing two alternating opaque-transparent Ronchi gratings (Khan, 2001) or two projected light patterns.

In this work, the imaging device itself plays the role of one of the grating with its regular 2D repetitive arrangement of charged-coupled cell arrays. This camera is then used to observe another grating. The interaction between the two 'gratings' results in the formation of Moiré patterns, which can be simply captured by the CCD camera itself. This imaging device-based approach of using Moiré fringes for surface displacement measurement was suggested by (Chang, 2003), where they demonstrated how wavelet transform (WT) could be used to extract the pitch of the Moiré fringes for micro-range measurement. A micro-pitch grating of 300 lines per inch (lpi) was employed as the specimen grating so that the pitch dimensions of the grating is close to that of the CCD cell spacing. This situation produces Moiré fringe patterns (see Fig. 2) that do not suffer annoying artufacts, making it relatively easy to extract the peak-to-peak fringe pitch. Unfortunately, peak-to-peak pitch values are only useful in providing distance measurements of flat surfaces perpendicular to the imaging plane. Their approach cannot be readily used to generate a dense varying depth map of the surface.

We propose using specimen grating with relatively larger pitch ($\leq$33 lpi), which can be easily printed with a 600 dpi laser printer. Unfortunately, such coarse pitch result in Moiré patterns that contain high frequency artifacts (see Fig. 3b), which embeds the desired Moiré fringe waveform. We discuss some property resulting from employing the CCD array as a reference grating that allows these artifacts to be easily removed. We also present a spatial domain model-fitting algorithm for measuring the instantaneous pitch width of the Moiré fringes, thus allowing the reconstruction of dense depth profiles.

2 THE MOIRÉ PATTERNS

2.1 Near Similar Pitch Gratings

Let the pitch width of the reference and specimen gratings be p_r and p_s respectively. In Fig. 1(a), we have a situation where the pitch of $p_s > p_r$, but only slightly. As a result, lower frequency Moiré fringes (light) with period p_m results due to the repeated and

Tu T. and Goh W. (2009).
MOIRÉ PATTERNS FROM A CCD CAMERA - Are They Annoying Artifacts or Can They be Useful? .
In *Proceedings of the Fourth International Conference on Computer Vision Theory and Applications*, pages 51-58
DOI: 10.5220/0001807700510058

regular maximum overlap of the two sets of dark lines. Dark fringes are observed in zones of minimum overlap. Assuming no relative rotation between the two line gratings, the Moiré fringe pitch, p_m is given by the well known equation [6]

$$p_m = \frac{p_r \times p_s}{|\, p_r - p_s \,|} \tag{1}$$

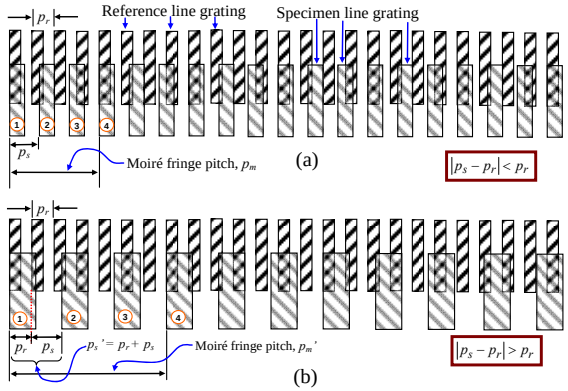

Figure 1: Resulting pitch for the Moiré fringes generated when the specimen grating pitch is (a) only slightly larger than the reference grating pitch and (b) much larger than the reference grating pitch. Notice the Moiré fringe pitch is made up of k = 3 specimen grating pitches in both cases.

Assume the reference line grating is now replaced by a regular-pitched CCD imaging cells. Fig. 2a shows the resulting 1-D image intensity profile. Notice that the extracted period p_m of the Moiré fringe pattern can be easily obtained as there are no specimen line grating artifacts, as observed with the 300 lpi line gratings used in (Chang, 2003).

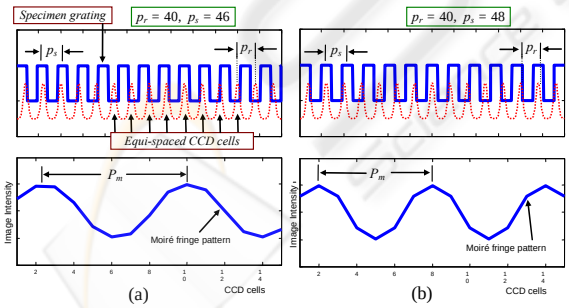

Figure 2: Moiré fringe patterns obtained when using point spread integration of the specimen grating intensity falling on regularly-spaced CCD cells. The image intensity profile obtained when the CCD pitch (reference grating) and the specimen line grating pitch are (a) p_r = 40, p_s = 46 and (b) p_r = 40, p_s = 48 spatial units respectively. As given in eqn. (1), the further p_r is from p_s, the narrower is the Moiré fringe pitch p_m.

2.2 Larger Pitch Gratings

What happens when the pitch of the specimen grating, p_s is much larger than that of the reference grating, p_r, as shown in Fig. 1b? We now derive a new expression for the Moiré fringe pitch, p_m' for the situation shown in Fig. 1b where $|p_s - p_r| > p_r$ since the fringe pitch expression given in eqn. (1) is only valid for the situations shown in Fig. 1a, where $|p_s - p_r| < p_r$. In order to make use of eqn. (1), we need to subtract the largest integer multiple of the reference pitch p_r from the large specimen line grating pitch p_s'. The remaining pitch value after subtraction, given by $\hat{p}_s$ is less than p_r and can therefore be substituted into eqn. (1) to compute the Moiré fringe pitch p_m. In Fig. 1b, we illustrate an example where this remaining pitch $\hat{p}_s$ is similar to the specimen grating pitch p_s in Fig. 1a. As shown in Fig. 1a, if the width of the Moiré fringe pitch p_m is made up of $k \times p_s$ width (example in Fig 1 has k = 3), then the fringe pitch p_m' of the wide specimen grating will also be given by $k \times p_s'$. From eqn. (1), the number of specimen line grating, p_s making up the Moiré fringe pitch width, p_m is given by

$$k = \frac{p_m}{p_s} = \frac{p_r}{p_r - p_s} \tag{2}$$

If $p_s' >> p_r$, we need to find the maximum number of integer multiples of p_r within p_s' given by

$$m = \left\lfloor \frac{p_s'}{p_r} \right\rfloor \tag{3}$$

where $\lfloor\ \rfloor$ is a flooring function. The remaining pitch $\hat{p}_s$ after removing multiples of p_r is given by

$$\hat{p}_s = p_s' - mp_r \quad \in [0, p_r] \tag{4}$$

The number of specimen line grating pitch width contained within the Moiré fringe pitch can be obtained by substituting (4) into (2), and is given by

$$k' = \frac{p_r}{p_r - \hat{p}_s} \tag{5}$$

We can now compute the Moiré fringe pitch, p_m' for the large specimen line grating with pitch p_s' from eqns. (4) and (5) and this is given by

$$p_m' = k' \times p_s' = \frac{p_r p_s'}{p_r - \hat{p}_s} = \frac{p_r p_s'}{(1+m)p_r - p_s'} \tag{6}$$

From this general expression of the Moiré fringe pitch, we can observe that the presence of the (1+m)

factor ensures that the absolute value of the denominator of both eqns. (1) and (6) will not exceed 1. This means the increase in specimen grating pitch p_s' will produce a fringe pitch p_m' that is equally magnified, as shown in Fig. 3b.

2.3 Removing Grating Artifacts

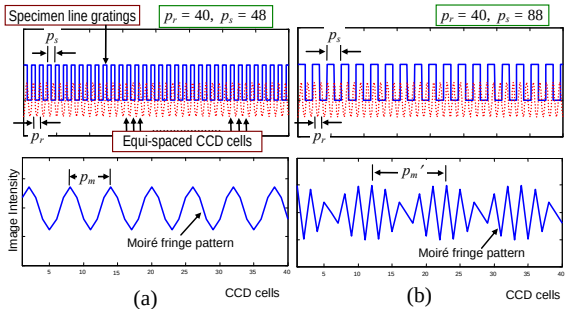

Figure 3: 1D Moiré fringe patterns obtained with specimen line gratings of different pitch widths. In both cases, the reference grating p_r = 40. Specimen line grating pitch in (a) p_s = 48 and in (b) p_s = 88, (i.e. $m = 1$). In both cases, the remaining pitch widths $\hat{p}_s = 8$.

The resulting Moiré pattern produced when $m > 1$ (see Fig. 3b) contains high frequency artifacts from the specimen line grating, which, makes automatic fringe pitch estimation difficult.

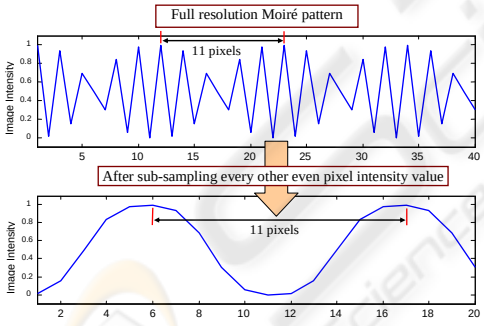

Figure 4: Removing line grating artifacts by sub-sampling. Notice the pitch width (i.e. 11 pixels) of the Moiré fringe remains unchanged after sub-sampling.

Since the reference grating pitch p_r is the pitch of the CCD cell and therefore the pixel width, we can quickly remove these high frequency artifacts by sub-sampling the Moiré pattern waveform as shown in Fig. 4. For situations where $m = 1$, down-sampling is done by selecting every other pixel in the original $N \times N$ sized image to form new image of size $N/2 \times N/2$. It is unimportant whether the even or the odd pixels are removed as this only results in a phase shift. When the value of $(1 + m)$ in eqn. (6) is 3, we can obtain an artifact-free waveform by sub-sampling every other 3rd pixel. When $(1 + m)$ is 4, we sub-sample every other 4th pixel and so on.

Given that the true pitch of the specimen grating is given by S. If we assume a thin lens (pin-hole) camera model and the distance of the surface of the specimen to the centre of projection given by d is relatively larger than the focal length of the camera given by f, the specimen grating pitch p_s' can be approximated by

$$p_s' = \frac{fS}{d} \tag{7}$$

Putting (7) into (6) and rearranging, we get

$$d = \frac{fS}{(1+m)}\left(\frac{1}{p_m'} + \frac{1}{p_r}\right) \tag{8}$$

Given that f, S, and p_r are constants, the distance d from the camera has an inversely proportional relation to the measure Moiré fringe pitch, p_m'.

2.4 CCD Cell Summation Model

The observed Moiré pattern is formed from the accumulation of individual CCD cell summation of the specimen line grating intensities. But how would the intensity summation model influence the shape of the resulting Moiré waveform? We obtained simulation results for three hypothetical summation models (see Fig. 5), namely impulse, Gaussian and uniform. Fig. 6 shows the resulting 1D Moiré pattern waveform for each of the summation models. Notice that the shape of the waveform is dependent on the CCD integration function but the fundamental frequency, which is related to the Moiré fringe pitch width, remains unchanged.

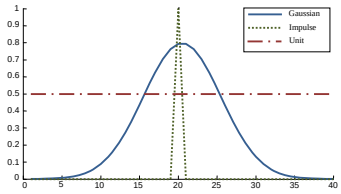

Figure 5: Three different intensity summation models for the hypothetical CCD cell.

From eqn. (8), the pitch period of the sub-sampled Moiré waveform provides a reciprocal description of the surface displacement d from the camera. As such, the instantaneous frequency (i.e. reciprocal of pitch) of the fundamental sinusoid of the waveforms shown in Fig. 6 will allow us to reconstruct a dense surface depth profile along a

selected 1D cross-section of the Moiré image. This is achieved independently of the assumed CCD cell summation model. We next describe an algorithm to extract the instantaneous frequency of a 1D sub-sampled Moiré pattern waveform.

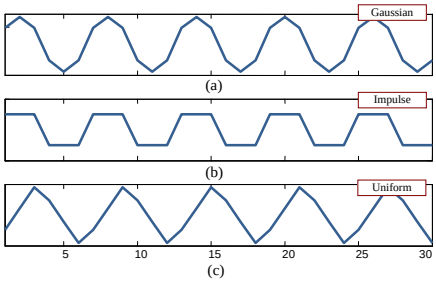

Figure 6: The resulting Moiré waveform using (a) Gaussian point spread, (b) impulse and (c) uniform CCD cell intensity summation model.

3 EXTRACTING DEPTH

Fig. 7(c) shows the sub-sampled waveform obtained from a 1D cross-section of a Moiré pattern image obtained for a curved line grating surface. The varying intensity could be due to shadows or uneven ambient lighting during imaging.

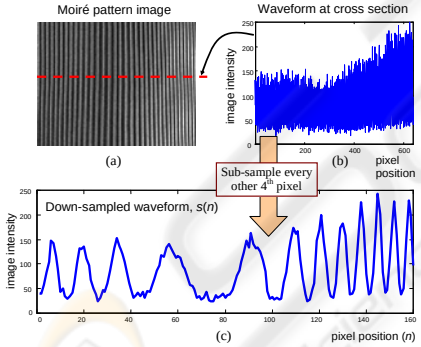

Figure 7: (a) Moiré pattern image of a curved line gating surface acquired under uneven lighting condition. (b) The full resolution intensity profile along the dotted (red) cross-section. (c) The waveform with the line grating artifact removed by sub-sampling every other 4th pixel in the original 1D cross section of the Moiré pattern image.

Notice that the sub-sampled waveform $s(n)$ in Fig. 7(c) can be viewed as a multi-component time-varying amplitude and frequency modulated (AM-FM) signal that is riding on a time-varying bias. In order, to extract the varying pitch period of the signal, we need to extract the instantaneous frequency of the fundamental sinusoid taking into account the varying bias and amplitude of the signal.

We modelled the fundamental AM-FM sinusoid by modifying the least-squares truncated power series approximation (L-STPSA) model approach of (Goh 2007) with an additional time-varying bias. Firstly, the sub-sampled waveform $s(n)$ is converted to a positive-negative going zero-mean signal $x(n)$ using

$$x(n) = s(n) - \frac{1}{N}\sum_{k=1}^{N} s(k) \tag{9}$$

3.1 The L-STPSA AM-FM Model

An AM-FM sinusoidal signal $\tilde{x}(n)$ with a varying bias given by $v(n)$ can be represented by

$$\tilde{x}(n) = A(n)\cos[w_c n + \theta(n)] + v(n) \tag{10}$$

where w_c is a fixed carrier frequency with varying amplitude $A(n)$. The instantaneous frequency $f(n)$ is the derivative of the varying phase $\theta(n)$ and is given by

$$f(n) = \frac{w_c + [d\theta(n)/dn]}{2\pi} \tag{11}$$

The signal $x(n)$ can be expanded to its in-phase and quadrature sinusoidal components given by

$$\tilde{x}(n) = a(n)\cos[w_c n + \theta(n)] + b(n)\sin[w_c n + \theta(n)] + v(n) \tag{12}$$

where $a(n)$ and $b(n)$ are given by

$$a(n) = A(n)\cos(\theta(n)) \text{ and } b(n) = -A(n)\sin(\theta(n)) \tag{13}$$

If we assume the functions that describe the varying amplitude $A(n)$ and phase $\theta(n)$ are analytic, then such functions can be approximated by a power series. As an example, cos x is given by the series

$$\cos x = 1 - x^2/2! + x^4/4! - x^6/6! + -... \tag{14}$$

We can now model the components of $\tilde{x}(n)$ and the varying bias $v(n)$ as general truncated power series of orders P and R respectively, given by

$$a(n) = \sum_{k=0}^{P} n^k a_k \;,\; b(n) = \sum_{k=0}^{P} n^k b_k \;,\; v(n) = \sum_{j=0}^{R} n^j v_j \tag{15}$$

The modelling process starts by assuming there are no phase variations (i.e. $\theta(n) = 0$). Then, given a signal $x(n)$ of sample length N, the modelled signal $\tilde{x}(n)$ in eqn. (10) can be estimated by minimising the mean squared-error ε in (16) with respect to the (P+1) pairs of amplitude coefficients, the (R+1) bias coefficients and predetermined carrier frequency w_c.

$$\varepsilon = \sum_{n=1}^{N} \{\tilde{x}(n) - x(n)\}^2 \tag{16}$$

Here, the coefficients estimation in (Goh, 1998) is extended with a further (R+1) equations to solve for the varying bias $v(n)$. Since the varying phase is estimated iteratively, it is not important what the predetermine carrier frequency w_c is as long as it is a frequency component present in the waveform. We chose w_c by picking the frequency corresponding to the highest peak frequency in the power spectrum of the waveform $x(n)$. (Goh, 2007) showed that the current estimate of the varying phase is given

$$\hat{\theta}(n) = \arctan\left[\frac{-b(n)\cos(\theta(n)) + a(n)\sin(\theta(n))}{a(n)\cos(\theta(n)) + b(n)\sin(\theta(n))}\right] \qquad (17)$$

From eqn. (15), both $a(n)$ and $b(n)$ can be estimated from the (P+1) a_k and b_k coefficients using the L-STPSA model of order P. With initial values of $\theta(n) = 0$, we make an initial estimate of the varying phase $\hat{\theta}(n)$ using eqn. (17). The phase is then unwrapped by tracking the 2π jumps in its values and then parameterised using another L-STPSA model of order Q given by

$$\theta(n) = \sum_{k=0}^{Q} c_k n^k \qquad (18)$$

The smooth L-STPSA reconstructed phase function $\theta(n)$ in (18) is then substituted back into the AM-FM signal model in (12) to obtain another new estimate of $a(n)$ and $b(n)$, which in turn is substituted, along with $\theta(n)$, into (17) to compute a new estimate of the varying phase $\hat{\theta}(n)$. This iterative parameter-substitution process is repeated until the waveform model in the Mth iteration deviates little from that estimated in the (M+1)th iteration. Fig. 8 shows the progressive sinusoidal signal estimation. For the waveform shown in Fig. 7(c), reasonable convergence occurred after the 6th iteration, with P = 12, Q = 5, R = 3 and w_c = 0.393.

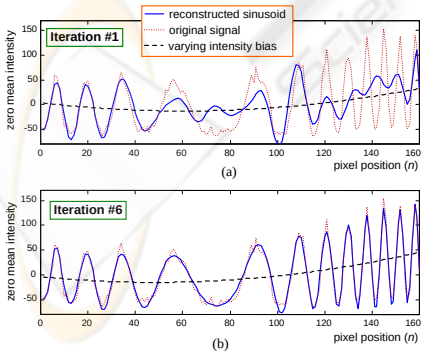

Figure 8: (a) The estimated L-STPSA AM-FM sinusoid of the fundamental frequency at (a) iteration #1 and (b) at stable full signal reconstruction at iteration #6. The original waveform and estimated varying bias is shown in dotted (red) and dashed lines (black) respectively.

Once a stable AM-FM sinusoid has been iteratively estimated, the varying phase $\theta(n)$ from (18) can yield an instantaneous frequency as given in (11). Since we are interested in the varying pitch period of the Moiré pattern, we can relate the varying phase $\theta(n)$ in (18) to the reciprocal of the Moiré pattern pitch width p_m' in (8) using the instantaneous frequency given in (11)

$$\frac{1}{p_m'(n)} = f(n) = \frac{w_c + \theta(n) - \theta(n-1)}{2\pi} \qquad (19)$$

The derivative of the varying phase in (11) is approximated using backward difference. Fig. 9 shows a 1D depth profile of the line grating surface shown in Fig. 7(a), obtained from the plot of $1/p_m'(n)$ in (19) using the fundamental sinusoid's estimated phase changes shown in Fig. 8(b).

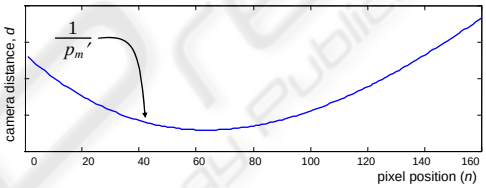

Figure 9: The cross-sectional profile of the distance between surface and camera computed from the instantaneous frequency estimate of the recovered L-STPSA sinusoidal signal in Fig. 8(b).

4 EXPERIMENTAL RESULTS

4.1 Experimental System Setup

The experimental setup used is shown in Fig. 10. It consists of a CCD camera mounted on a crank-based height-adjustable stand, a personal computer (PC) and A4-sized white paper with uniform black-white line gratings printed from a 600dpi laser printer. The camera is the Dragon Fly Express monochrome model (PointGrey, 2008) from Point Grey Research Inc., with a C-mount lens of focal length 25mm. The resolution of the captured image is 640 × 480 pixels.

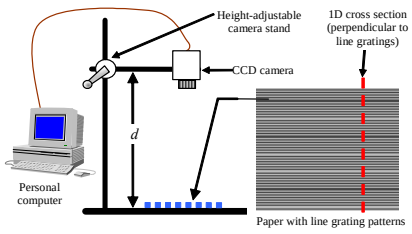

Figure 10: The basic experimental setup.

The distance, d from the camera imaging plane to the line grating surface is proportional to the inverse of Moiré fringe pitch width, $1/p_m'$ and this width is related to the instantaneous frequency of the Moiré waveform as shown in (19). In other words, the 1D distance profile along the cross section shown in Fig. 10 can be generalized to

$$d(n) = k \times \frac{1}{p_m'(n)} + b = kf(n) + b \qquad (20)$$

where k and b are unknown system constants. The instantaneous frequency $f(n)$ given in (19) is computed from the extracted L-STPSA fundamental sinusoid of the 1D Moiré pattern waveform.

The first experiment verifies that the distance from the camera, d is proportional to the extracted instantaneous frequencies, f of the fundamental sinusoid of the 1D Moiré pattern waveform. The L-STPSA model parameter values of $P = 5$, $R = 3$ and $Q = 2$, as given in eqns. (15) and (18) was used. By setting $Q = 2$, we are adopting a constant phase model as we do not expect the frequency of the Moiré pattern to change over the 1D cross section since the distance, d to the surface is much larger that the focal length, f of the camera lens.

Fig. 11 shows the results obtained for the d distances from 70.0cm to 75.0cm, in steps of 0.5cm. At this distance and with the printed line grating pitch used, the value of m in (3) is 3 and artifact-free 1D Moiré waveform is obtained by sampling every other 4th pixel of the original resolution waveform. Notice that the results obtained in Fig. 11 confirm the proportional relationship given in (20).

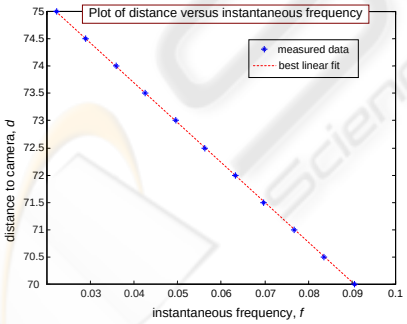

Figure 11: A plot to show the relationship between the distance, d between the line grating surface and the CCD camera and the estimated instantaneous frequency, f of the Moiré pattern waveform.

4.2 1D Incline Planar Surfaces

This experiment demonstrates the use of the AM-FM modelling property of the L-STPSA technique to estimate the changing instantaneous frequency of the Moiré pattern waveform across the 1D cross section. By using an incline line grating surface, the distance to the camera would vary linearly from one end of the 1D cross section (see Fig. 12) to the other.

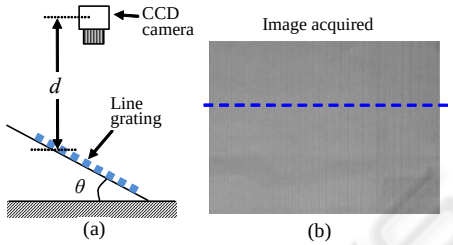

Figure 12: (a) Experimental setup for the incline planar surface analysis. (b) The acquired image with the dashed line (blue) indicating the 1D profile used in the analysis.

Fig. 13(a) shows the Moiré pattern waveform obtained for a planar incline of about 10 degrees. Fig. 13(b) shows the corresponding frequency-varying fundamental sinusoid estimated using the L-STPSA model parameters of $P = 5$, $R = 3$ and $Q = 5$. The linearly changing chirp-like instantaneous frequency fundamental sinusoid can be seen in the Moiré waveform shown in Fig. 13(b).

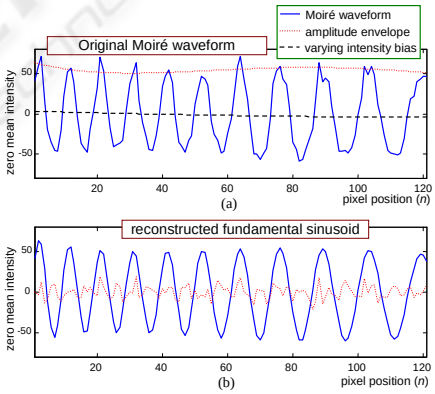

Figure 13: (a) The Moiré pattern waveform obtained from an incline line grating. Also shown is the estimated amplitude envelope for the fundamental sinusoid and the varying bias. (b) The extracted fundamental sinusoid of the Moiré waveform using the L-STPSA modelling technique. Shown in dotted line (red) is the error residue between the estimated sinusoid and the original signal in.

Fig. 14 shows the plot of the instantaneous frequency of the fundamental sinusoid in Fig. 13(b). Observe that the extracted instantaneous frequency varies closely to that of an incline, as we would expect from the proportional relationship between distance, d and instantaneous frequency, f in (20).

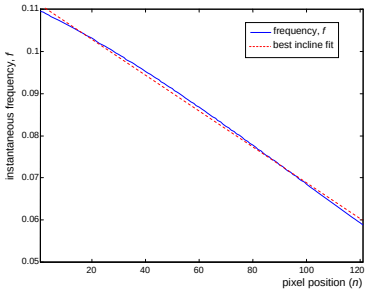

Figure 14: The incline observed in the instantaneous frequency, f is plotted against a best fit incline.

4.3 2D Incline Planar Surfaces

Next, we imaged a line grating surface that is inclined in both the x and y directions (see Fig. 15). We reconstructed a dense surface depth map by stitching together the all perpendicular 1D cross sections across the image. Fig. 16 shows the resulting dense 2D depth map reconstructed by analysing a series of 1D cross sections.

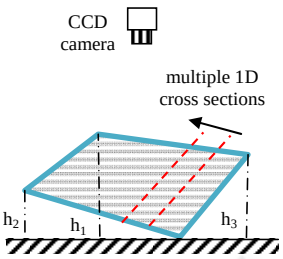

Figure 15: The 2D incline surface experimental setup. The heights h_1 =64.5 mm, h_2 =37mm, and h_3 =33mm.

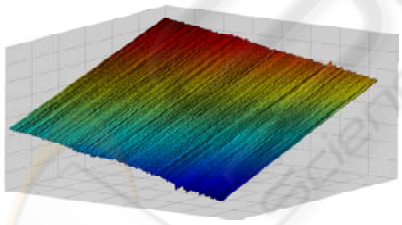

Figure 16: Reconstructed 2D surface of the incline plane.

4.4 Impact of Uneven Lighting Conditions

We studied the effects of ambient lighting variations on the accuracy of the extracted depth using the proposed CCD Moiré waveform analysis technique. Fig. 17 shows the setup used in which a curved A4-sized paper with evenly spaced vertical line gratings was imaged twice. Firstly, under normal lighting conditions and secondly, with portions of the line grating surface covered by shadows.

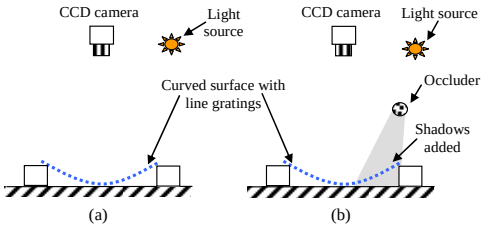

Figure 17: Experimental setup for testing effects of lighting variations. (a) Normal light source and (b) Shadows cast on surface due to partially occluded light source.

Fig. 18 shows the two waveforms obtained after sub-sampling the intensity value of every other 4th pixel of a 1D cross section. The fundamental sinusoidal waveforms along with their respective instantaneous frequencies were extracted for both waveforms using $P = 10$, $Q = 5$ and $R = 3$. The carrier frequencies used in Fig. 18(a) and 18(b) were $w_c = 0.668$ and $w_c = 0.628$ respectively.

The resulting 1D depth profiles of the surface cross section under different lighting conditions were plotted together as shown in Fig. 19. Hardly any noticeable variations in depth profiles were observed. This shows that the proposed technique for measuring the depth profile of a line grating surface is robust to lighting variations. The ability of the L-STPSA technique to simultaneously extract the varying instantaneous frequency and amplitude modulation envelopes in a waveform allows us to handle changes in the Moiré pattern intensity, which does not fundamentally change the pitch of the Moiré fringes.

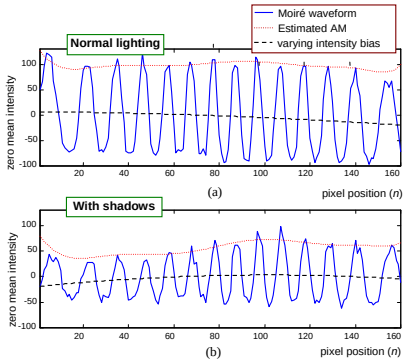

Figure 18: The 1D intensity profiles of the sub-sampled zero-mean Moiré pattern waveforms obtained under (a) normal lighting condition and (b) with shadows. Notice the shadows resulted in uneven intensity attenuation. The estimated amplitude modulation envelopes of the

fundamental sinusoids are shown dotted (red) and the varying biases are shown in dashed lines (black).

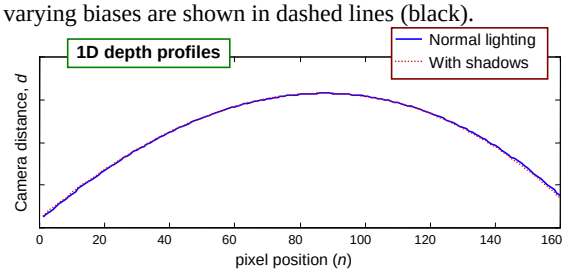

Figure 19: The plot of the two estimated 1D depth profiles of Moire pattern waveforms in Figure 19(a) and 19(b). The two overlapping profiles are almost identical despite the significant variation in the intensity profile.

5 CONCLUSIONS

We introduced a method of measuring dense 2D surface depth maps using the Moiré patterns captured from a CCD camera. This uniform CCD cell array is exploited in the generation of the Moiré patterns, making this approach simpler and less expensive than the use of Ronchi gratings. A novel sub-sampling technique was introduced to remove artifacts that resulted from adopting a more convenient and inexpensive setup in which larger specimen line grating pitch width were be employed.

A spatial domain parametric technique was proposed for extracting the instantaneous frequency of the Moiré pattern waveform and we showed that this frequency parameter is proportional to the surface-camera distance and can therefore be used to analyse the relative depth variation of the line grating surface. We also showed that the depth profiles estimated from the observed Moiré pattern are independent of the intensity variations over the line grating pattern, which makes such measurement techniques easy to deploy under conditions that consistent and uniform lighting cannot be assured.

REFERENCES

Kafri, O., Glatt, I., 1990, *The Physics of Moiré Metrology*, John Wiley & Sons.

Khan, A. S., Wang X., 2001, *Strain Measurements and Stress Analysis*, Prentice Hall, New Jersey.

Walker, C.A. (Ed), 2004, *Handbook of Moiré Measurement*, Institute of Physics Publishing, Bristol.

Creath, K., Schmit, J., Wyant, J.C., 2007, Optical Metrology of Diffuse Surfaces. In *Optical Shop Testing*, Malacara, D. (Ed.), John Wiley & Sons, Hoboken, New Jersey, 3rd edition, pp. 756-807.

Chang, R. S., Sheu, J.Y., Lin C.H., Liu H.C., 2003, Analysis of CCD Moiré Pattern for Micro-range measurements using the Wavelet Transform. *Optics and Laser Technology* (35) pp. 43-47.

Amidror, I., 2000, *The Theory of the Moiré Phenomenon*, Kluwer Academic Publishers, Dordrecht, The Netherlands.

Goh, W. B., 2007, Noise Robust AM-FM Demodulation using Least-Squares Truncated Power Series Approximation. In *ICICS'07, 6th Intl. Conf. on Information, Communications and Signal Processing.*

Goh, W. B., Chan, K.Y., 1998, Amplitude Modulated Sinusoidal Modeling using Least-square Infinite Series Approximation with Applications to Timbre Analysis. In *ICASSP'98, IEEE Intl. Conf. of Acoustics, Speech and Signal Processing*, (6), pp. 3561-3564.

Point Grey Research Inc., 2008, Dragonfly Express, http://www.ptgrey.com/products/dx/dx.pdf